JOURNAL OF SOLID STATE CHEMISTRY 139, 266–273 (1998)
ARTICLE NO. SC987840

Microscopic Studies on $Y_2Ba_4Cu_7O_{15-\delta}$ by Use of TEM and NQR Techniques

Masaki Kato,*,[1] Makoto Nakanishi,*,[2] Toshio Miyano,† Tadashi Shimizu,‡ Masato Kakihana,§ Kazuyoshi Yoshimura,* and Koji Kosuge*

*Division of Chemistry, Graduate School of Science, Kyoto University, Kyoto 606-01, Japan; †Department of Science, Maizuru College of Technology, 234 Shiraya, Maizuru-city 625, Japan; ‡National Research Institute for Metals, 3-13 Sakura, Tsukuba-shi 305, Japan; and §Materials and Structures Laboratory, Tokyo Institute of Technology, 4259 Nagatsuta, Midori-ku, Yokohama 226, Japan

Received December 8, 1997; in revised form March 27, 1998; accepted April 2, 1998

$Y_2Ba_4Cu_7O_{15-\delta}$ compounds were characterized by microscopic investigation using TEM and NQR techniques. We synthesized Y247 compounds by two kinds of preparation methods: the conventional solid-state reaction (sample A) and the polymerized-complex method (sample B). The value of T_c for sample A was found to be 65 K and that for sample B was 93 K by ac-χ measurements. As a result of TEM experiments, stacking faults along the *c* axis were observed more frequently in sample B than in sample A. These stacking faults resulted in microdomains containing pure Y123 or Y124 thin blocks of several unit cells. NQR experiments revealed that the microscopic environment of Cu(2) sites in sample A differed from either of those in the Y123 and Y124 compounds. NQR frequency values (ν_Q) of Cu(2) sites agreed well with those calculated by the point charge model applied for the Y247 structure. The spectra of Cu(2) sites in sample B could be regarded, however, as a combination of those of pure Y123, Y124, and also Y247 compounds. This fact was coincident with the result of TEM experiments. We concluded that the superconductivity of Y247 with higher T_c originates from the thin block of Y123.

I. INTRODUCTION

Since the discovery of high-T_c cuprate superconductors, $Y_2Ba_4Cu_{6+n}O_{14+n}$ phases ($n = 0$, 1, and 2) have attracted much interest with respect to their chemical and physical properties as a prototype of high-T_c superconductivity. The $Y_2Ba_4Cu_7O_{15-\delta}$ (Y247) phase has a crystal structure consisting of alternative intergrowth of $YBa_2Cu_3O_{7-\delta}$ (Y123, $T_c = 93$ K) and $YBa_2Cu_4O_8$ (Y124, $T_c = 82$ K), containing single and double Cu–O chains along the *b* axis, respectively (1–4). Hence the Y247 compound can be regarded as a multilattice of two superconductors. It is, however, an open question that two maximum values of T_c, the vicinity of 90 K and 60 K, have been reported for Y247 compounds (5–8). These compounds could not be distinguished each other by X-ray powder diffraction patterns. Therefore, one can consider that the difference should be caused by the difference in the microstructures of these two compounds. Several authors have reported transmission electron microscopy (TEM) investigations of Y247 compounds with different values of T_c (9, 10). They concluded that the lower T_c in Y247 compounds should be due to stacking faults along the *c* axis. However, those stacking faults result in the disordered arrangement of the Y123 and Y124 blocks, implying that individual CuO_2 planes remain in each block. Unfortunately, theoretical models of interplane coupling between CuO_2 planes have not been established so far.

Stern *et al.* reported detailed nuclear quadrupole resonance (NQR) and nuclear magnetic resonance (NMR) investigations of Y247 compounds with T_c of 95 K (11–13). In their report (13), they clearly indicated the evidence for the interlayer coupling between CuO_2 double layers using NQR spin-echo double resonance (SEDOR). NQR measurement is useful in observing the microscopic environment around nuclei from the viewpoint of resonance frequency (ν_Q), which can be estimated from the atomic coordination. Hence, it is interesting to investigate the difference in the microscopic environments between these Y247 compounds by NQR experiments.

Recently, we characterized Y247 compounds by TEM and NQR techniques (14, 15). As a result, we derived the opposite conclusion that the Y247 phase with higher T_c contains more stacking faults than that with lower T_c. In this paper, using TEM and NQR measurements, we report the microscopic characterization of Y247 compounds with different T_c values obtained by the two kinds of preparation methods. In the following section, experimental details are presented. In Section III, we present results of (a) the ac-χ

[1]To whom correspondence should be addressed.

[2]Present address: Department of Applied Chemistry, Faculty of Engineering, Okayama University, 3-1-1 Tsushimanaka, Okayama 700, Japan.

0022-4596/98 $25.00

measurement to confirm superconducting properties of two kinds of Y247 samples, (b) direct observation of the microscopic structure using TEM technique, and (c) analysis of the microscopic environment from the viewpoint of NQR frequency. The origin of superconductivity in these Y247 compounds is also mentioned in this section. Concluding remarks are given in the last section.

II. EXPERIMENTAL

Polycrystalline compounds of Y247 were synthesized by means of the conventional solid-state reaction and the polymerized-complex method. The procedure for the solid-state reaction was as follows (sample A). The raw materials of Y_2O_3, $BaCO_3$, and CuO of 99.99% purity were mixed thoroughly, pelleted, and heated in air at 900 °C for 24 h to decarbonate. After this heating, we were able to obtain a composite sample consisting of Y123 and CuO phases. This sample was exposed to the heat treatment at 250 °C in flowing H_2 gas for 12 h. A key point for succeeding in preparation of pure Y247 phase is this heat treatment, which produces fine powders and promotes the following chemical reactions. Then, the sample was heated under 5-bar oxygen pressures at 950°C for 48 h in a quartz tube, in which liquid oxygen was trapped by using liquid nitrogen in advance. After this reaction, the quartz tube was quenched in water because the Y124 phase is known to be stable at low temperature. After this treatment, we annealed the sample in flowing O_2 gas at 350°C to obtain Y247 compound with $\delta \simeq 0$. In other procedure, the polymerized-complex method (sample B), Y247 samples were synthesized under 1 atm of O_2 gas. According to the phase diagram reported in the early stage (16, 17), the Y247 phase should be unstable in such an atmosphere. Although revised phase diagrams were reported (18, 19), we can consider that the successful synthesis by this method was due to the reactive precursor in which the cation could be distributed uniformly by the polymerization. For details of procedures, refer to Ref. (20). To reduce the oxygen content in samples A, we successively annealed them in flowing N_2 gas for 2 days in the range 650 to 700 °C. As a result, we obtained Y247 samples of various oxygen contents, $0 \leq \delta \leq 1$.

The samples obtained were characterized by X-ray diffraction (XRD) measurements using monochromatic Cu$K\alpha$ radiation.

The oxygen content $15 - \delta$ was measured electrochemically by the coulometric titration method. This method was first applied for high-T_c Bi-based oxides by Kurusu *et al.* (21) to distinguish the valences of copper and bismuth. We used copper (I) chloride (CuCl) as a reducing reagent in this method. Then, we followed procedures similar to those of Kurusu *et al.* One should refer to their report and related papers (22, 23) for details.

The ac susceptibility (ac-χ) was measured by the Hartshorn method for powdered samples soaked in paraffin for insulation among powder particles.

The microstructure for samples A and B was investigated with JEOL100-CX and 2010-F transmission electron microscopes.

NQR experiments were performed by the spin-echo pulse sequence mode using a homemade spectrometer. Spectra for ^{63}Cu and ^{65}Cu nuclei were taken under zero external magnetic field. Two peaks should be observed for one Cu site, including isotopes of ^{63}Cu and ^{65}Cu, due to the quadrupole interaction without the long-range magnetic order in the sample.

III. RESULTS AND DISCUSSION

3.1. Characterization and ac-χ Measurements

Both samples A and B were characterized by XRD experiments. They were found to be single phases of Y247. Lattice parameters for samples A and B were $a = 3.841$ Å, $b = 3.877$Å, $c = 50.47$ Å and $a = 3.835$ Å, $b = 3.872$ Å, and $c = 50.43$ Å, respectively. From the coulometric titration method, the δ values were found to be 14.98 for sample A and 14.92 for sample B. As a result of XRD measurement and coulometric titration, we could not distinguish samples A and B clearly.

The T_c values for samples A and B, however, were found to be different. We show the results of ac-χ measurements of samples A and B in Fig. 1. The T_c value for sample A was around 65 K and that for sample B was 93 K, although the

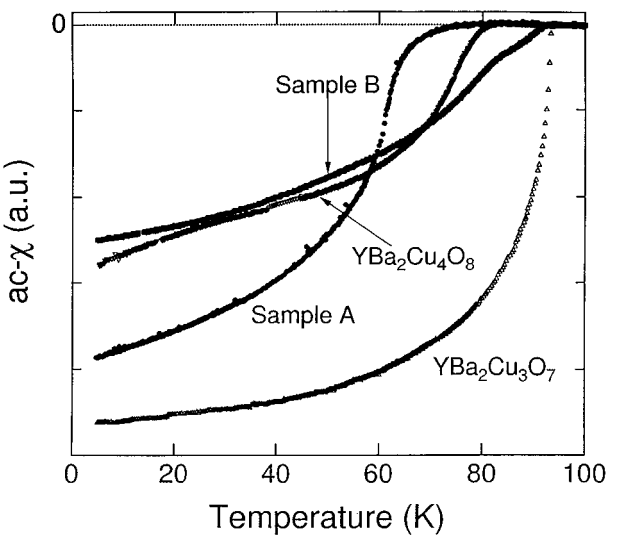

FIG. 1. Temperature dependence of ac-χ for $YBa_2Cu_3O_7$, $YBa_2Cu_4O_8$ and samples A and B of $Y_2Ba_4Cu_7O_{15}$. For ac-χ measurement, powdered samples were soaked in paraffin to exclude the proximity effect between particles.

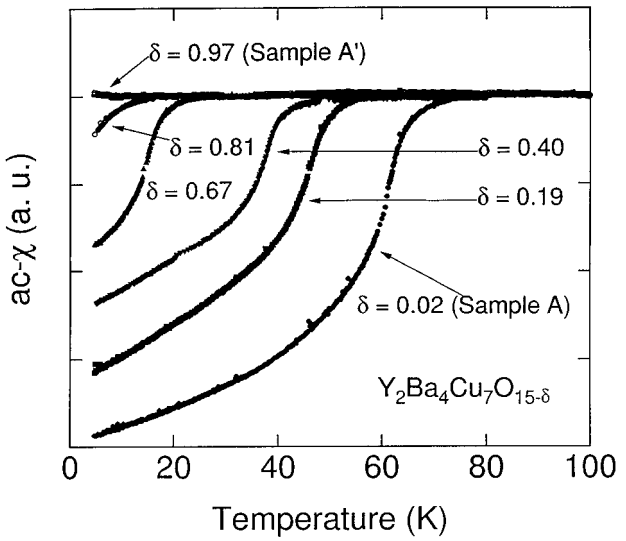

FIG. 2. Temperature dependence of ac-χ for samples A with various oxygen contents.

oxygen contents of both samples were almost the same. Sample B shows a relatively sharp superconducting transition compared with sample A, while sample B has the lower Meissner fraction. One can note that superconducting characteristics of both samples are obviously not good as Y123 nor Y124 phases, from the viewpoint of the sharpness at the transition and the superconducting fraction. In Fig. 2, we also show the temperature dependence of ac-χ for samples A with various oxygen deficiencies δ. The values of T_c and the Meissner fraction decreased with increasing oxygen deficiency δ. Moreover, superconductivity almost disappeared for the sample of $\delta = 0.97$ (sample A′). In Fig. 3,

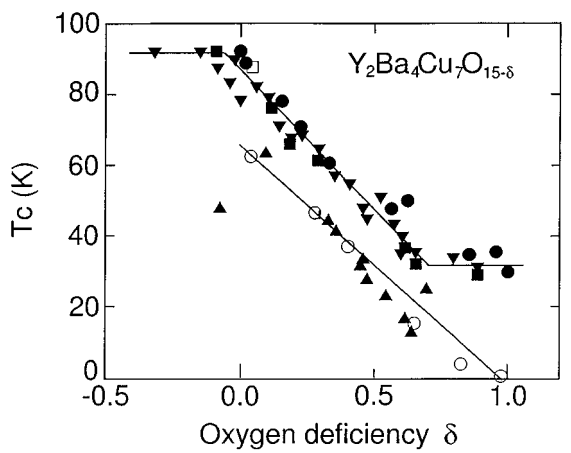

FIG. 3. Oxygen content dependence on T_c of Y247 compounds. Data of several groups are plotted in addition to our samples A (○) and B (□). ▲, ●, ■, and ▼ correspond to the data of Karpinski *et al.* (5), Tallon *et al.* (6), Triscon *et al.* (7), and Genoud *et al.* (8), respectively.

this oxygen content dependence of sample A on T_c is summarized together with results of several other groups (5–8). One can note that the δ dependence of samples with lower T_c at $\delta = 1$ (LT sample) is different from that of samples with higher T_c (HT sample). Though all samples show nearly the same value of $dT_c/d\delta$, HT samples have a superconductivity with $T_c = 15$ K even at $\delta = 1$. As mentioned above, superconductivity disappears when δ in sample A is 1. From the electric resisitivity measurement using the conventional four-probe method, this most deoxidized sample of Y247 showed metallic conductivity down to 4.2 K without the superconducting transition. We discuss the relation between metallic conductivity and microstructure below.

It is noted that the difference in T_c values should be caused by the difference in the microstructures of those two compounds. We can consider mainly two reasons: (a) occupancies of oxygen in the single CuO chain sites and (b) stacking faults along the c axis owing to the disordered arrangement of Y123 and Y124 blocks. As for (a), neutron diffraction measurements were reported by several workers for Y247 compounds with various values of T_c (9, 24). According to them, site occupancies perpendicular to the b axis were in the range 32 to 46% for samples with $\delta \simeq 0$ independent of T_c. It may be concluded that the difference in T_c values is not due to reason (a).

3.2. TEM Observations

To elucidate the difference in microscopic structure, especially with respect to reason (b), TEM experiments were done for both samples A and B. We have succeeded in observing microscopic structures for some particles of samples A and B. First, we show typical electron diffraction (ED) patterns with [100] zone axis for both samples in Fig. 4a and 4b. Diffraction spots along the c^* axis correspond to a d space of about 50 Å, which agrees with the lattice parameter of c axis for Y247 compounds. Sample A shows a sharp diffraction pattern, although sample B exhibits some streaks along c^* axis. As a result of observing some specimens, we can conclude that most of the ED patterns for sample B exhibit such streaks, in contrast to those for sample A. We show typical lattice images for samples A and B in Fig. 5. In Fig. 5a, dark and bright fringes are located with two different alternating spaces of 11.6 and 13.7 Å which almost coincide with the c lattice parameter for Y123 and half of that for Y124. One can also observe partial displacements that upset the regular sequence –S–D–S–D– along the c axis, to produce a stacking fault such as –S–D–S–S–D–, where S and D correspond to single and double Cu–O chain blocks. The result is then a microblock of Y123 or Y124. We show a high-resolution image for another specimen of sample A in Fig. 5b. The area in this figure almost can be regarded as the Y247 structure,

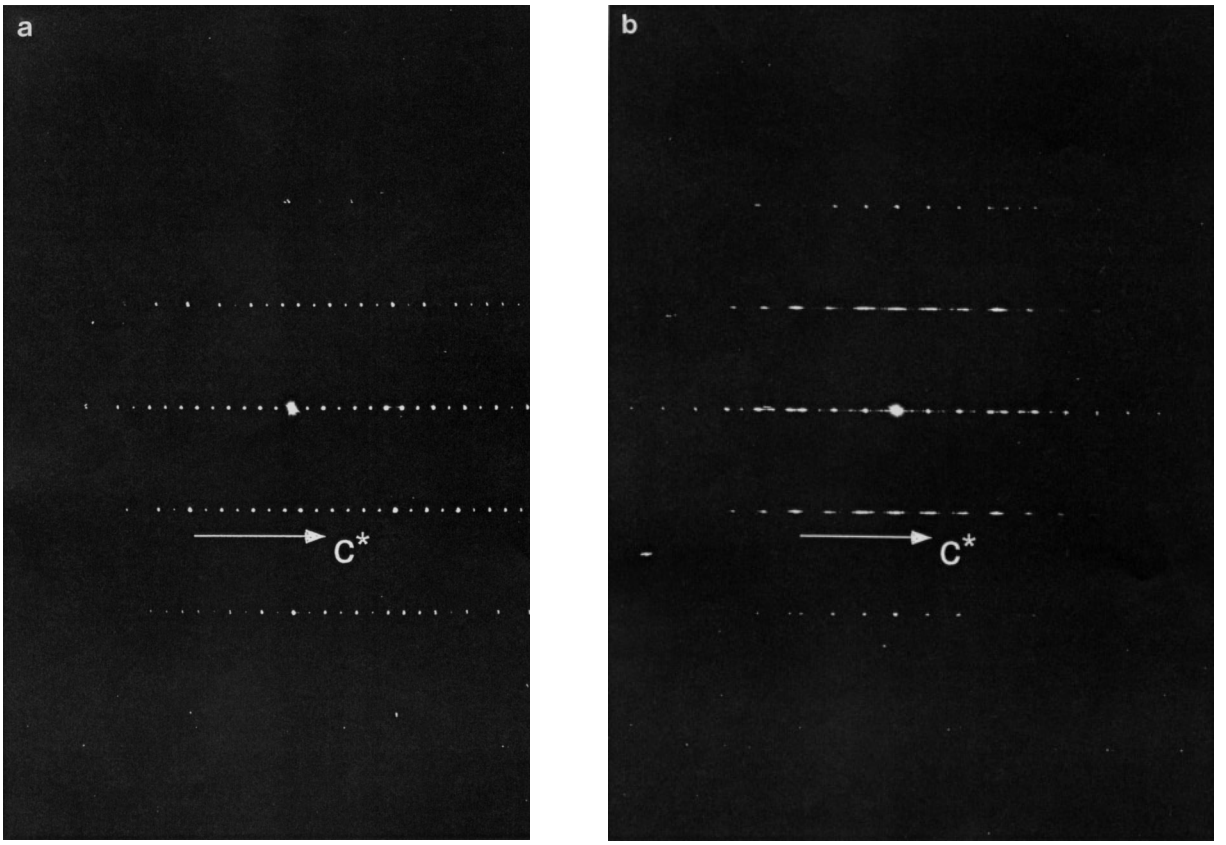

FIG. 4. Electron diffraction patterns with [100] zone axis for Y247 samples of A (a) and B (b).

although a few stacking faults can be observed as shown by the arrows. In Fig. 5c, we show a magnified image for the selected area indicated in Fig. 5b. Note the complete Y247 structure in these lattice fringes arranged in two alternative rows. On the other hand, some stacking faults, consisting of Y123 or Y124 thin blocks with a size of several unit cells, can be observed in Fig. 5d. We also present an image for another specimen of sample B and the magnified one in Figs. 5e and 5f, respectively. In Fig. 5f, note Y123, Y247, and Y124 microdomains in regions I, II, and III. As a result, for sample B, we could find successive single or double chains with spacing of the c parameter for Y123 or a half for Y124 phase, respectively. These six images are typical ones as a consequence of statistical observations for about 30 specimens of each sample of A and B. We have, therefore, confirmed that the differences in microstructure between samples A and B are significant and that these stacking faults along the c axis are observed more frequently within sample B than sample A.

Here, let us discuss qualitatively the relation between microstructure and metallic conductivity, i.e., nonsuperconductivity, of sample A′ ($\delta = 1$). From the experiment for Y123 thin films, Bando *et al.* reported that only a single layer of CuO_2 showed the superconducting transition under limiting conditions (25, 26). In sample A′, although oxygen at single-chain sites is almost removed, Y1248 blocks remain without oxygen deficiency and have adequate contents of holes to show superconductivity. Hence, from the fact that no superconducting transition was observed in sample A′, we may conclude that the interlayer coupling between CuO_2 layers should play an intrinsic role in quenching superconductivity in this compound. Assuming that the interlayer coupling has the tendency to suppress superconductivity, we can consider that sample A′ has fewer stacking faults along the direction of coupling, c axis, which is consistent with the results of TEM experiments for sample A. This may also be noted from the fact that Y1236 blocks in sample A′ do not show long-range antiferromagnetic order due to the interlayer coupling as indicated by the NQR experiment described below.

Several groups have recently reported TEM investigations of Y247 compounds with different T_c values (9, 10). They claimed that Y247 samples with a T_c of 95 K should have fewer stacking faults than those with lower T_c, contrary to our conclusion. Berastegui *et al.* investigated two Y247 samples with T_c of 95 and 89 K using high-resolution

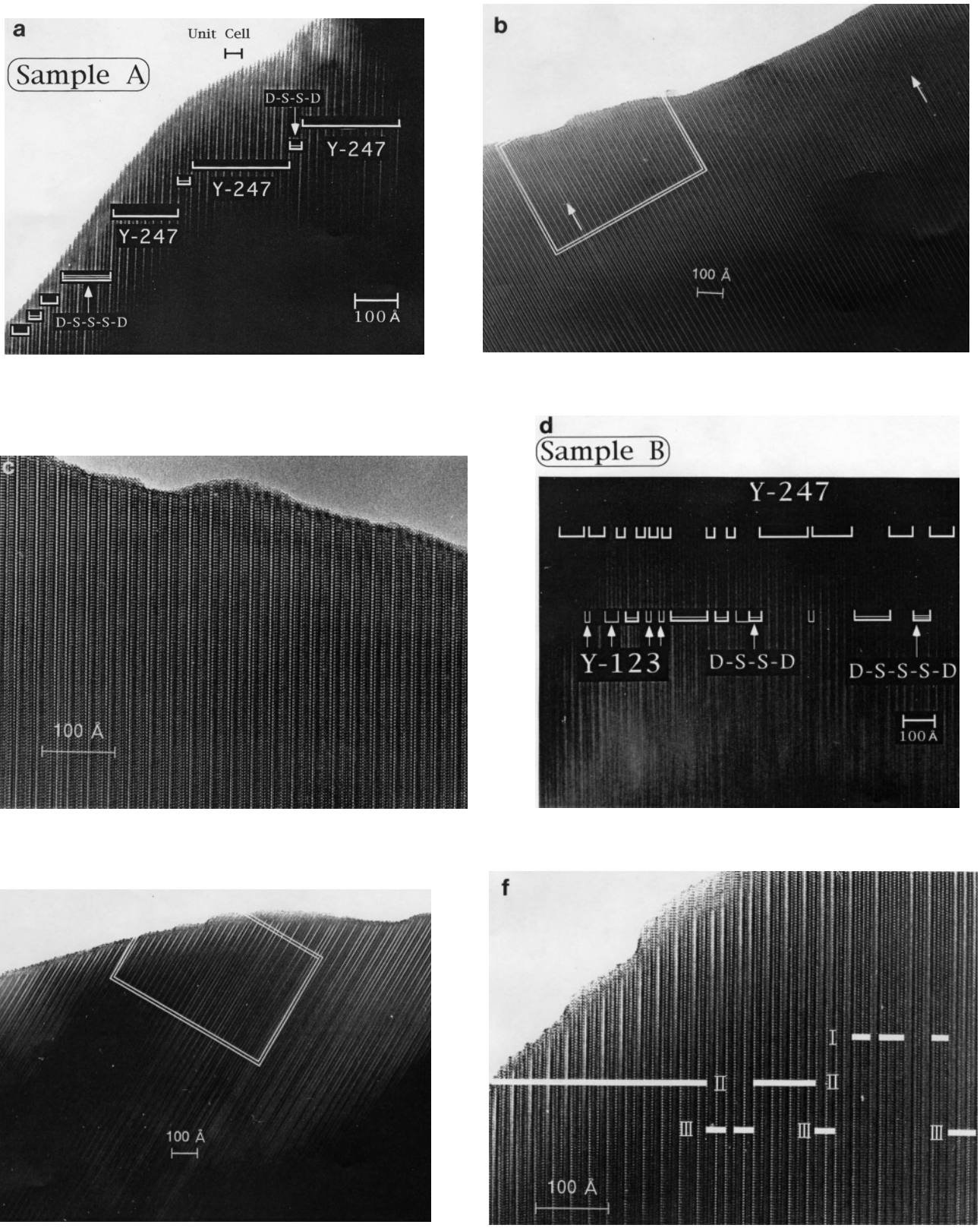

FIG. 5. Typical TEM images for the samples A (a–c) and B (d–f). Images (a) and (b) were obtained by JEOL 100-CX and the others by JEOL 2010-F. Selected areas in (b) and (e) correspond to images (c) and (f), respectively. S and D indicate single and double Cu–O chains (a, b). I, II, and III denote Y123, Y247, and Y124, respectively (f).

neutron diffraction and TEM (9). However, both of their samples were synthesized by polymerized-complex method, as was our sample B. Thus, both of them had frequent stacking faults and a higher T_c than our sample A. Guo *et al.* also investigated two differently processed Y247 samples by TEM technique (10). Values of T_c for those two samples were reported to be 95 and 80 K, and those samples were obtained by the solid-state reaction. The sample with a T_c of 80 K showed two distinct transitions at 80 and 56 K. In the case of our sample A, two similar transitions were sometimes observed, although those samples exhibited XRD patterns typical of a Y247 single phase. Considering the phase diagram (16–19) and the value of T_c onset ($= 80$ K), we can ascribe the reason for those two transitions to the existence of Y124 microdomains, which should be caused by incomplete quenching after the heat treatment. On the other hand, the TEM image for their sample with higher T_c also showed dislocations with a (001) glide plane. Considering the effect of interlayer coupling as mentioned above, the higher T_c of these phases cannot be regarded as an intrinsic character of Y247 compounds.

3.3. NQR Experiments

As a clue to elucidating the microscopic environment and the role of stacking faults, Cu-NQR measurements were made on these Y247 compounds. In Fig. 6, we show NQR spectra for Y123 (a), Y124 (b), samples A and B of Y247 with $\delta \simeq 0$ (c and d), and sample A′ with $\delta \simeq 1$ (e) measured at 1.3 K. The spectra with NQR frequency (ν_Q) around 20 MHz can be attributed to Cu(1) sites and those with ν_Q around 30 MHz to Cu(2) sites, as previously reported (11, 27–29). Here, the Cu(1) and Cu(2) sites mean the Cu on CuO (single or double) chain and CuO_2 plane sites, respectively. As mentioned above, two peaks should be observed for one Cu site if the compound does not have long-range magnetic order. From the spectra for sample A′ in Fig. 6e, also CuO_2 planes in $Y_2Ba_4Cu_7O_{14}$ phase do not have magnetic order as in other superconducting Y–Ba–Cu–O systems.

The difference between samples A and B can clearly be seen in the spectra of Cu(2) sites in Figs. 6c and 6d. For sample A, one can find spectra consisting of two peaks, the widths of which are about twice as broad as those of Y123 or Y124. In the ideal Y247 structure, there exist two Cu(2) sites from the crystallographic viewpoint: one is near the single chain and the other is near the double chain. Hence, the broadness of the spectra can be explained by the result of the superposition of NQR spectra due to these two Cu(2) sites with the similar ν_Q around 30 MHz, as shown in Fig. 7a. Because the value of ν_Q for sample A was intermediate between those of Y123 and Y124 compounds, it can be concluded that the microscopic state of Cu(2) sites should be different from either of those in the Y123 and Y124 compounds. For sample B, however, the spectra of Cu(2) site can

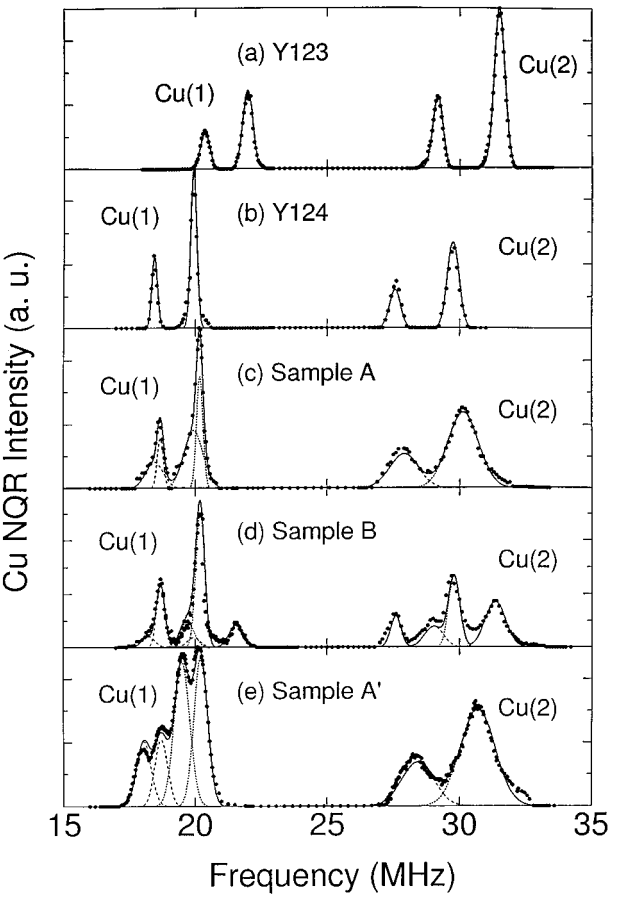

FIG. 6. NQR spectra for Y123 (a), Y124 (b), and samples A (c), B (d), and A′ (e) measured at 1.3 K. Solid circles and solid lines correspond to experimental data and fitted line, respectively. Dotted and broken lines also indicate components for ^{63}Cu and ^{65}Cu, respectively, which were obtained by curve fitting.

be explained by the combined spectra of Y123, Y124, and sample A, as shown in Fig. 7b, which suggests the presence of microdomains of Y123 and Y124 in the Y247 matrix.

Here, let us show what kinds of physical properties determine the value of ν_Q. Without an applied or an internal static magnetic field, an NQR signal can be observed at the frequency

$$\nu_Q = \frac{3e^2qQ}{2I(2I-1)h}, \qquad [1]$$

where eq is the electric field gradient (EFG) tensor ($eq = V_{zz}$), Q the nuclear quadrupole moment, I the nuclear spin, I being 3/2 for ^{63}Cu and ^{65}Cu nuclei, and h Planck's constant. In this equation, the asymmetry parameter η is neglected since it is recognized to be essentially zero for planar Cu sites. Therefore, the value of ν_Q must be deduced from the value of eq. It is commonly known that the total value of eq consists of two components: the first component

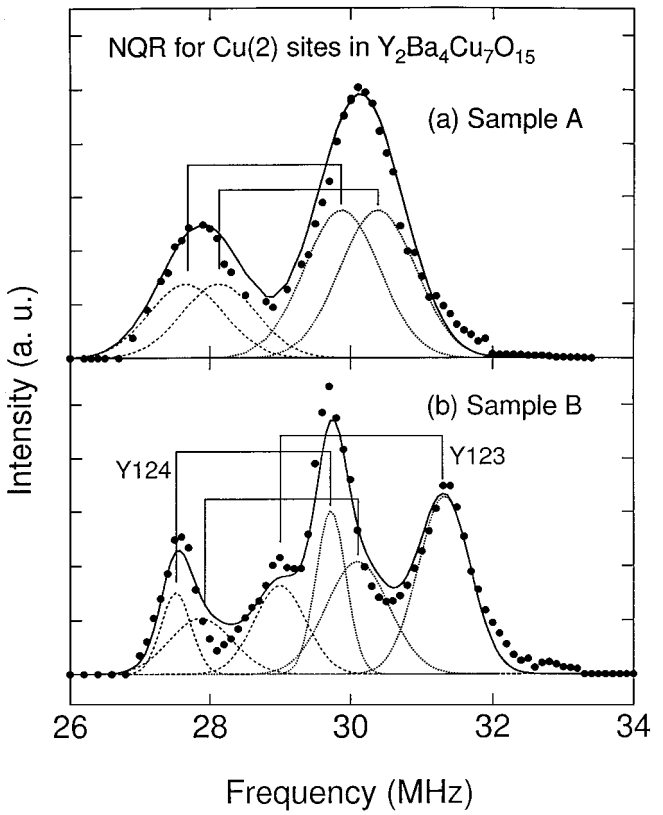

FIG. 7. NQR spectra for Cu(2) sites in samples A and B. Dotted and broken lines indicate components for ^{63}Cu and ^{65}Cu, respectively. Pairs of $^{63}\nu_Q$ and $^{65}\nu_Q$ for each site are also shown.

is due to the direct lattice EFG (eq_{latt}) and the second arises from the EFG caused by the nonfilled shells of the ion itself (eq_{nfs}). In the point charge model, eq_{latt} is given by

$$eq_{\text{latt}} = \sum_i \frac{e_i(3z_i^2 - r_i^2)}{r_i^5}, \qquad [2]$$

where the sum is over all lattice points and e_i is the charge of the ith ion. For a variety of Cu oxides including high-T_c oxides, T. Shimizu, one of the present authors, has derived a clear correlation between the experimental value of ν_Q and the value of eq_{latt} calculated by the point charge model (30, 31). This empirical law can be written as

$$\nu_Q = a \cdot eq_{\text{latt}} + b, \qquad [3]$$

a and b being constants independent of materials. Assuming Eq. [3] is also applicable to Y247 compounds, ν_Q should be obtained by calculating the value of eq_{latt}.

At first, using the point charge model, we estimated values of ν_Q for ^{63}Cu nuclei ($^{63}\nu_Q$) at two kinds of Cu(2) sites to be 29.87 and 30.52 MHz. These values agreed well with the experimental values for sample A as shown in Fig. 7a, where the spectra were successfully decomposed into two components with $^{63}\nu_Q$ of 29.90 and 30.33 MHz. In the point charge model, the value of eq_{latt} was found to be convergent if the radius, in which the summation of EFG from surrounding atoms (Eq. [2]) was carried out, was more than 50 Å. Therefore, from the close agreement between observed and calculated values of ν_Q for sample A, we can consider sample A to have almost perfect Y247 structure within any ranges with a radius of about 50 Å. On evaluation of ν_Q for the Y247 compound, the charge of holes on CuO_2 planes was pushed into the uniform increase in the charge of oxygen. Nevertheless, success in the simple ionic model may be considered as the tendency for cancellation between contributions of the covalency to eq_{latt} and to eq_{nfs}, as mentioned in the literature (30). Moreover, this consideration is clearly proved by our results of the direct observation using TEM as mentioned above.

On the other hand, the result of NQR spectra for sample B in Fig. 7b can be regarded as the existence of microdomains consisting of Y123, Y124, and also Y247 structure with the size of several unit cells, according to Shimizu's empirical correlation. Note that this result also agrees with TEM experiments for sample B. Stern *et al.* have reported detailed NQR and NMR investigations for Y247 compounds with T_c of 95 K (11–13). In their report (13), they clearly indicated the evidence for the interlayer coupling beteen CuO_2 double layers using NQR spin-echo double resonance. Their NQR spectra, however, can be recognized to be the same as those for our sample B. In their report, the value of ν_Q was not analyzed theoretically, although observed values of ν_Q were assigned to each copper site on the basis of their similarity in the spectrum profile or in the temperature dependence of ν_Q and T_1 to those of Y123 and Y124 compounds. The structural characterization of their samples is anticipated.

Finally, we discuss why the higher value of T_c could be achieved in sample B. As a result of TEM and NQR measurements, we can conclude that the superconductivity with T_c of 93 K for sample B was attributed to microdomains with Y123 structure. We may consider the superconductivity in the Y123 thin blocks to be possible on the basis of the short coherence length of 31 Å along the c axis. Several groups, however, have reported higher T_c values for the Y247 phase than for the Y123 phase (6, 8). Guo *et al.* reported that a T_c of 95 K for a Y247 sample can be regarded as a result of some chemical strains due to dislocations with Burger vectors along the [100] and [110] directions (10). From any viewpoint, it should be difficult to distinguish the effect of the chemical pressure due to dislocation from that owing to stacking faults, although they insisted that stacking faults along the c axis have the negative effect on the value of T_c. In fact, it has not been established theoretically how interlayer coupling and/or uniaxial chemical pressure affect the value of T_c.

Nevertheless, from our experiments, we suspect that higher values of T_c may be caused by chemical strain due to stacking faults.

IV. CONCLUSION

$Y_2Ba_4Cu_7O_{15-\delta}$ compounds were characterized by microscopic investigation using TEM and NQR techniques. As a result of TEM experiments, disordered intergrowth structures consisting of stacking faults along the *c* axis were observed more frequently in sample B with a T_c of 93 K than in sample A with a T_c of 65 K. These stacking faults result in microdomains containing Y123 or Y124 blocks with a size of several unit cells. As a result of NQR experiments, the local environment of the Cu(2) site in sample A was found to differ from either of those in the Y123 and Y124 compounds. For sample B, however, the spectra of the Cu(2) site were analyzed to be the superposition of those of Y123, Y124, and sample A, which suggests the presence of thin blocks of Y123 and Y124. We conclude that the superconductivity of Y247 with a T_c of 93 K can be attributed to the existence of Y123 thin blocks in the sample.

ACKNOWLEDGMENTS

The authors are grateful to Mr. T. Ohmura and Mr. H. Kato for their kind help in the experiments. The authors are also indebted to Mr. M. Suzuki for his assistance in TEM experiments. This work was partially supported by a Grant-in-Aid for Scientific Research from the Ministry of Education, Science, Sports and Culture of Japan.

REFERENCES

1. P. Bordet, C. Chaillout, J. Chenavas, J. L. Hodeau, M. Marezio, J. Karpinski, and E. Kaldis, *Nature* **334,** 596 (1988).
2. C. Beeli, H. U. Nissen, Y. Kawama, and P. Stadelmann, *Z. Phys. B* **73,** 313 (1988).
3. C. Chaillout, P. Bordet, J. Chenavas, J. L. Hodeau, M. Marezio, J. Karpinski, E. Kaldis, and S. Rusiecki, *Solid State Commun.* **70,** 275 (1989).
4. T. Krekels, G. van Tendeloo, S. Amelinckx, J. Karpinski, S. Rusiecki, E. Kaldis, and E. Jilek, *Physica C* **178,** 383 (1991).
5. J. Karpinski, S. Rusiecki, B. Bucker, E. Koldis, and E. Jilek, *Physica C* **161,** 618 (1989).
6. J. L. Tallon, D. M. Pooke, R. G. Buckley, M. R. Presland, and F. J. Blunt, *Phys. Rev. B* **41,** 7220 (1990).
7. G. Triscone, J.-Y. Genoud, T. Graf, A. Junod, and J. Müller, *Physica C* **201,** 1 (1992).
8. J.-Y. Genoud, T. Graf, G. Triscone, A. Junod, and J. Müller, *Physica C* **192,** 137 (1992).
9. P. Berastegui, P. Fischer, I. Bryntse, L.-G. Johansson, and A. W. Hewat, *J. Solid State Chem.* **127,** 31 (1996).
10. Y. X. Guo, R. Høier, T. Graf, and J.-Y. Genoud, *Philos. Mag. B* **72,** 383 (1995).
11. R. Stern, M. Mali, I. Mangelschots, J. Roos, and D. Brinkmann, *Phys. Rev. B* **50,** 426 (1994).
12. R. Stern, M. Mali, J. Roos, and D. Brinkmann, *Phys. Rev. B* **51,** 15478 (1995).
13. R. Stern, M. Mali, J. Roos, and D. Brinkmann, *Phys. Rev. B* **52,** 15734 (1995).
14. M. Kato, T. Ohmura, M. Nakanishi, T. Miyano, K. Yoshimura, T. Kakihana, and K. Kosuge, *in* "Proceedings, International Symposium on Metallurgy and Materials of Non-ferrous Metals and Alloys," p. 388 (1996).
15. M. Kato, H. Kato, T. Ohmura, M. Nakanishi, T. Miyano, K. Yoshimura, M. Kakihana, and K. Kosuge, *in* "Advances in Superconductivity XI" (S. Nakajima, Ed.). Springer-Verlag, Tokyo, 1997.
16. D. E. Morris, N. G. Asmar, J. H. Nickel, R. L. Sid, and J. Y. T. Wei, *Physica C* **159,** 287 (1989).
17. J. Karpinski, S. Rusiecki, E. Kaldis, B. Bucher, and E. Jilek, *Physica C* **160,** 449 (1989); **161,** 618 (1989).
18. E. Kaldis, J. Karpinski, S. Rusiecki, B. Bucher, K. Conder, and E. Jilek, *Physica C* **185–189,** 190 (1991).
19. J. Karpinski, K. Conder, H. Schwer, Ch. Krüger, E. Kalis, M. Maciejewski, C. Rossel, M. Mali, and D. Brinkmann, *Physica C* **227,** 68 (1994).
20. P. Berastegui, M. Kakihana, M. Yoshimura, H. Mazaki, H. Yasuoka, L.-G. Johansson, S. Eriksson, L. Borjesson, and M. Kall, *J. Appl. Phys.* **73,** 2424 (1993).
21. K. Kurusu, H. Takami, and K. Shintomi, *Analyst* **114,** 1341 (1989).
22. M. Karppinen, H. Yamauchi, and S. Tanaka, *J. Solid State Chem.* **104,** 276 (1993).
23. M. Karppinen, A. Fukuoka, J. Wang, S. Takano, M. Wakata, T. Ikemachi, and H. Yamauchi, *Physica C* **208,** 130 (1993).
24. A. W. Hewat, P. Fischer, E. Kalis, J. Karpinski, S. Rusiecki, and E. Jilek, *Physica C* **167,** 579 (1990).
25. T. Terashima, K. Shimura, Y. Bando, Y. Matsuda, A. Fujiyama, and S. Komiyama, *Phys. Rev. Lett.* **67,** 1362 (1991).
26. K. Shimura, Y. Daitoh, Y. Yano, T. Terashima, Y. Bando, Y. Matsuda, and S. Komiyama, *Physica C* **228,** 91 (1993).
27. T. Shimizu, H. Yasuoka, T. Imai, T. Tsuda, T. Takabatake, Y. Nakazawa, and M. Ishikawa, *J. Phys. Soc. Japan* **57,** 2494 (1988).
28. C. H. Pennington, D. J. Durand, D. B. Zax, C. P. Slichter, J. P. Rice, and D. M. Ginsberg, *Phys. Rev. B* **37,** 7944 (1988).
29. H. Zimmermann, M. Mali, I. Mangelschots, J. Roos, D. Brinkmann, J. Karpinski, S. Rusiecki, and E. Kaldis, *J. Less-Common Met.* **164/165,** 132 (1990).
30. T. Shimizu, *J. Phys. Soc. Japan* **62,** 772 (1993).
31. T. Shimizu, *J. Phys. Soc. Japan* **62,** 779 (1993).